

Structure-based inhibitor design for evaluation of a CYP3A4 pharmacophore model

Parminder Kaur, Richard Chamberlin, Thomas L. Poulos, and Irina F. Sevrioukova

J. Med. Chem., **Just Accepted Manuscript** • DOI: 10.1021/acs.jmedchem.5b01146 • Publication Date (Web): 15 Sep 2015

Downloaded from <http://pubs.acs.org> on September 16, 2015

Just Accepted

“Just Accepted” manuscripts have been peer-reviewed and accepted for publication. They are posted online prior to technical editing, formatting for publication and author proofing. The American Chemical Society provides “Just Accepted” as a free service to the research community to expedite the dissemination of scientific material as soon as possible after acceptance. “Just Accepted” manuscripts appear in full in PDF format accompanied by an HTML abstract. “Just Accepted” manuscripts have been fully peer reviewed, but should not be considered the official version of record. They are accessible to all readers and citable by the Digital Object Identifier (DOI®). “Just Accepted” is an optional service offered to authors. Therefore, the “Just Accepted” Web site may not include all articles that will be published in the journal. After a manuscript is technically edited and formatted, it will be removed from the “Just Accepted” Web site and published as an ASAP article. Note that technical editing may introduce minor changes to the manuscript text and/or graphics which could affect content, and all legal disclaimers and ethical guidelines that apply to the journal pertain. ACS cannot be held responsible for errors or consequences arising from the use of information contained in these “Just Accepted” manuscripts.

1
2
3
4
5
6
7
8
9
10
11 **Structure-based inhibitor design for evaluation of a CYP3A4 pharmacophore**
12
13 **model**
14
15
16
17
18
19
20
21

22 Parminder Kaur^{†§}, A. Richard Chamberlin^{†‡}, Thomas L. Poulos^{†·‡·¶} and Irina F.
23 Sevrioukova^{¶*}
24
25
26
27
28

29 [†]Departments of Pharmaceutical Sciences, [‡]Chemistry and [¶]Molecular Biology and
30 Biochemistry, University of California Irvine, California, 92697, United States
31
32
33
34
35
36
37
38
39
40
41
42
43
44
45
46
47
48
49
50
51
52
53
54
55
56
57
58
59
60

Abstract

Human cytochrome P450 3A4 (CYP3A4) is a key xenobiotic-metabolizing enzyme that oxidizes and clears the majority of drugs. CYP3A4 inhibition may lead to drug-drug interactions, toxicity and other adverse effects but, in some cases, could be beneficial and enhance therapeutic efficiency of co-administered pharmaceuticals that are metabolized by CYP3A4. Based on our investigations of analogs of ritonavir, a potent CYP3A4 inactivator and pharmacoenhancer, we have built a pharmacophore model for a CYP3A4-specific inhibitor. This study is the first attempt to test this model using a set of rationally designed compounds. The functional and structural data presented here agree well with the proposed pharmacophore. In particular, we confirmed the importance of a flexible backbone, the H-bond donor/acceptor moiety and aromaticity of the side group analogous to Phe-2 of ritonavir, and demonstrated the leading role of hydrophobic interactions at the sites adjacent to the heme and phenylalanine cluster in the ligand binding process. The X-ray structures of CYP3A4 bound to the rationally designed inhibitors provide deeper insights into the mechanism of the CYP3A4-ligand interaction. Most importantly, two of our compounds (**15a** and **15b**) that are less complex than ritonavir have comparable sub-micromolar affinity and inhibitory potency for CYP3A4 and, thus, could serve as templates for synthesis of second generation inhibitors for further evaluation and optimization of the pharmacophore model.

Introduction

Cytochrome P450 3A4 (CYP3A4) is the most abundant and clinically relevant xenobiotic-metabolizing enzyme in humans. CYP3A4 catalyzes diverse oxidative reactions and is involved in the metabolism of endogenous steroids, the majority of administered drugs and other foreign molecules, such as environmental pollutants, carcinogens, pesticides and insecticides.¹⁻⁸ CYP3A4 has a large and malleable active site that accommodates a wide variety of molecules, some of which could inhibit or enhance metabolism. *In vivo*, CYP3A4 inhibition has a greater impact on human health, as it can lead to xenobiotic-induced toxicity and drug-drug interactions, one of the reasons for late-stage clinical trial failures and withdrawal of marketed pharmaceuticals.

However, carefully controlled CYP3A4 inhibition can be beneficial and is currently exploited in the treatment of HIV infection. To date, two CYP3A4 inhibitors, ritonavir and cobicistat (Fig. 1), are marketed as pharmacoenhancers for the HIV-1 protease inhibitors that serve as substrates for CYP3A4.⁹⁻¹³ Both drugs were developed based on chemical structure/activity relationships studies rather than the CYP3A4 crystal structure. Moreover, ritonavir was originally designed to inhibit the HIV-1 protease,¹⁴ whereas its ability to potently inactivate CYP3A4 was coincidental and discovered later.⁹ Cobicistat is a derivative of ritonavir that lacks the backbone hydroxyl group, critical for binding to catalytic Asp25 and Asp225 of HIV-1 protease, and has a morpholine ring instead of the valine side group (Fig. 1). As a result, cobicistat is not an anti-HIV protease inhibitor so its prolonged usage does not promote the development of drug-resistant HIV strains. Also, this pharmaceutical has fewer side effects and better physico-chemical properties, yet is comparable but not superior to ritonavir in terms of

1
2
3 inhibitory potency for CYP3A4.¹²
4

5
6 There is no general agreement on the CYP3A4 inhibitory mechanism of ritonavir.
7
8 Several groups suggested that ritonavir is a mechanism-based inactivator,¹⁵⁻¹⁹ whereas
9
10 others argued against the mechanism-based CYP3A4 inhibition²⁰ and concluded that
11
12 ritonavir acts as a competitive²¹ or a mixed competitive-noncompetitive CYP3A4
13
14 inactivator.²²⁻²⁴ Our data on highly purified recombinant CYP3A4 do not support the
15
16 mechanism-based or competitive type of inhibition as a predominant inactivation
17
18 pathway and rather suggest that ritonavir inactivates CYP3A4 *via* strong thiazole
19
20 nitrogen coordination to both ferric and ferrous CYP3A4 which decreases the heme
21
22 redox potential and impedes electron transfer from the redox partner, cytochrome P450
23
24 reductase.²⁵ This conclusion is well supported by the X-ray structures of CYP3A4
25
26 complexed with ritonavir and 10 ritonavir analogs.²⁵⁻²⁸ Most importantly, the
27
28 accumulated functional and structural data enabled us to identify several important
29
30 trends in the ligand binding process and define strategies for rational, structure-based
31
32 inhibitor design.²⁹ In particular, we found that: (i) strong binding through the heme-
33
34 ligating moiety is a prerequisite for potent CYP3A4 inhibition, and pyridine possesses
35
36 more favorable stereoelectronic properties for the heme ligation than any other chemical
37
38 groups tested; (ii) the flexible backbone enables a better fit into the CYP3A4 active site;
39
40 (iii) the side group at a Phe-2 position (indicated in Fig. 1) is critically important because
41
42 it not only fills the hydrophobic cavity (P2 site) but also has a potential to stabilize the
43
44 protein-ligand complex *via* different types of interactions with the heme-ligating group
45
46 and nearby Arg105; (iv) occupation of the pocket hosting the Phe-1 group (P1 site) is
47
48 also important and greatly improves inhibitory potency; (v) polar interactions with
49
50
51
52
53
54
55
56
57
58
59
60

1
2
3 Ser119 increase the ligand affinity and association rate, regardless of whether the
4 hydrogen bond with the ligand is established or not; and (vi) the terminal group
5 modulates the CYP3A4-inhibitor complex affinity and stability which, in turn, correlate
6 with the ligand-induced changes in the melting temperature and the amplitude of the
7 442 nm absorption of the ferrous ligand-bound form.
8
9

10
11
12
13
14
15 Previous 3D-pharmacophores for drug metabolism prediction were built based on
16 P450 homology and quantitative structure-activity relationship (QSAR) modeling
17 because the X-ray structure of CYP3A4 was not available at that time.³⁰⁻³³ In addition,
18 there is no structure-based inhibitor pharmacophore that could assist in identification
19 and early elimination of potential CYP3A4 inactivators during development of drugs and
20 other chemicals relevant to public health. Having mapped the inhibitory determinants
21 within the CYP3A4 active site, we were able to build a pharmacophore model for a
22 CYP3A4-specific inhibitor (Fig. 2).²⁹ Our strategy for the model evaluation was to
23 synthesize and analyze ritonavir-like molecules using a general scaffold (Fig. 3) where
24 the pyridine ring serves as a heme-ligating moiety and the remainder of the inhibitor is
25 stitched together with units containing various side and terminal groups (R_1 - R_3). By
26 systematically changing R_1 - R_3 substituents, it can be probed how each chemical moiety
27 contributes to the binding affinity and inhibitory potency, and how CYP3A4 adapts to
28 changes in the ligand's structure.
29
30
31
32
33
34
35
36
37
38
39
40
41
42
43
44
45
46
47

48 Here we present structural and functional results on the first set of commercially
49 available and rationally designed pyridine-containing compounds that differ in the
50 backbone length and R_2 substituents (Fig. 4). With this initial set, we were able to
51 confirm the importance of a flexible backbone, aromaticity of the R_2 group and the H-
52
53
54
55
56
57
58
59
60

1
2
3 bond donor/acceptor moiety (pharmacophoric determinants II, III and V), as well as the
4
5 leading role of hydrophobic interactions at the P1 and P2 sites in the ligand binding
6
7 process.
8
9

10 11 12 **Results and Discussion**

13
14
15 *Inhibitor Design* – As mentioned in the Introduction, both CYP3A4 inhibitors currently
16
17 marketed as pharmacoenhancers, ritonavir and cobicistat (Fig. 1), were developed
18
19 based on chemical structure/activity relationships studies rather than the CYP3A4
20
21 crystal structure. Ritonavir is a large peptidomimetic drug designed to inhibit an HIV-I
22
23 protease,⁹ whereas cobicistat was developed through ritonavir derivatization.^{13, 34}
24
25
26
27 Synthesis of both compounds is a complex process requiring production of specific
28
29 stereoisomers. To evaluate our pharmacophore model, we decided to build CYP3A4
30
31 inhibitors from scratch using a general simple scaffold (Fig. 3) where the modules
32
33 containing the side and terminal groups (R_1 , R_2 and R_3) are linked to the heme-ligating
34
35 pyridine *via* a flexible backbone. Pyridine and aminoethylpyridine (Fig. 4) were obtained
36
37 from Sigma-Aldrich. The rationale for designing compounds **4**, **5**, **11** and **15a-b** was to
38
39 determine how elongation of the backbone, introduction of the H-bond donor/acceptor
40
41 (peptide bond), and substitution of R_2 affect affinity, inhibitory potency and the ligand
42
43 binding mode. Mass spectrometry and NMR data for compounds **4-15a/b** are included
44
45 in the Supporting Information section.
46
47
48
49

50
51
52
53 *Binding Affinity and Association Kinetics* – Addition of pyridine, aminoethylpyridine and
54
55 compound **5** to CYP3A4 led to a decrease and a small red shift (~2 nm) in the Soret
56
57
58
59
60

1
2
3 band (Fig. 5). Spectral dissociation constants (K_s) for pyridine and aminoethylpyridine
4
5 were in the millimolar range (Table 1), whereas **5** had two binding sites with K_s of 10 μ M
6
7 and 4.4 mM. Compounds **4**, **11** and **15a-b**, on the other hand, bind to a single site and
8
9 induce a notable shift in the Soret band, typical for type II ligands (Fig. 6). Introduction of
10
11 the hexane or phenyl side group increased the binding affinity by 10- and 100-fold,
12
13 respectively, relative to **4**. The phenyl-to-indole substitution led to a further decline in K_s
14
15 (by ~2-fold; Table 1). Another important feature is a pronounced 442 nm absorption of
16
17 the ferrous **15a**- and **15b**-bound forms of CYP3A4. The corresponding 442 nm peak
18
19 was considerably smaller for the CYP3A4-**4/11** complexes and undetectable for the
20
21 pyridine-, aminoethylpyridine- and **5**-bound forms (Figs. 5 and 6). In our previous
22
23 studies,²⁵⁻²⁸ we found that the amplitude of the 442 nm band of the ferrous species
24
25 correlates with the inhibitory potency of the ligand, in that compounds whose binding led
26
27 to a higher 442 nm absorption peak were acting as more potent CYP3A4 inactivators
28
29 (e.g., ritonavir and pyridine-substituted desoxyritonavir (GS3; Fig. 1)). Therefore, a
30
31 significant but not complete conversion to the 442 nm absorbing species taking place
32
33 upon association of CYP3A4 with **15a** and **15b** was the first indication that these
34
35 compounds may have a comparable although not superior inhibitory potency relative to
36
37 GS3 and ritonavir.
38
39
40
41
42
43
44
45

46 The binding reactions of CYP3A4 with pyridine, aminoethylpyridine and **5** were
47
48 monophasic, with rate constants of 0.5-0.8 s⁻¹. In contrast, association with **4**, **11** and
49
50 **15a-b** proceeded in two phases. The rate constant for the fast phase (k_{fast}) was the
51
52 highest for **4** and the lowest for **15a** (20 and 1.7 s⁻¹, respectively; Table 1). Notably, k_{fast}
53
54 for **15a** was close to that of ritonavir (1.4 s⁻¹)²⁵ and nearly 5-fold lower than the
55
56
57
58
59
60

1
2
3
4
5
6
7
8
9
10
11
12
13
14
15
16
17
18
19
20
21
22
23
24
25
26
27
28
29
30
31
32
33
34
35
36
37
38
39
40
41
42
43
44
45
46
47
48
49
50
51
52
53
54
55
56
57
58
59
60

respective value for **15b** and GS3. Together, the spectral and kinetic data suggest that (i) the backbone elongation and addition of a side group complicate the binding reaction, (ii) the presence of a bulky, hydrophobic R₂ group increases the ligand affinity but slows down the association rate, and (iii) indole as a R₂ substituent promotes complex formation with CYP3A4 to a higher degree than the hexane or phenyl rings.

Melting Temperature and Inhibitory Potency – None of the investigated compounds increased the thermal stability of CYP3A4, as evidenced by the lack of feasible ligand-dependent changes in melting temperature (ΔT_m ; Table 1). CYP3A4 T_m was slightly increased upon complex formation with **15b** but decreased in the presence of other compounds, most notably for the **11**- and **15a**-bound forms (by 1-2°C). This is in contrast to ritonavir and its analogs, whose ligation to CYP3A4 increases T_m by 2-7°C.^{27, 28} Nevertheless, a common trend revealed by thermal denaturation is an increase in thermostability of CYP3A4 upon association with ritonavir-like compounds. The heme ligation and occupation of the P1 and P2 cavities by hydrophobic moieties likely stabilize CYP3A4 by decreasing conformational flexibility.

As expected, the inhibitory potency of the investigated compounds on the BFC debenzoylation activity of CYP3A4 correlated with the binding affinity (Table 1). The IC₅₀ values were the highest for pyridine, aminoethylpyridine and **5** (1-4 mM), intermediate for **4** and **11** (75 and 30 μ M, respectively), and the lowest for **15a** and **15b** (0.5 and 0.2 μ M, respectively). Importantly, IC₅₀s for **15a** and **15b** were close to those for ritonavir and GS3 (0.55 and 0.13 μ M, respectively).²⁷ Thus, addition of only one aromatic side

1
2
3 group and *tert*-butyloxycarbonyl (*Boc*) as a terminal moiety transforms compound **5**, a
4
5 very weak ligand, into a potent CYP3A4 inactivator.
6
7

8
9
10 *Crystal Structures of the 15a- and 15b-bound CYP3A4* – We succeeded in co-
11
12 crystallization of CYP3A4 with **4**, **15a** and **15b**. Compound **11** dissociated from CYP3A4
13
14 during crystallization. Crystal structures of CYP3A4 ligated to **15a** and **15b** were
15
16 determined to 2.60 and 2.76 Å, respectively (Supporting Information Table 1S). Both
17
18 compounds bind to the active site and ligate to the heme iron through the pyridine
19
20 nitrogen (Fig. 7). The GS3-bound model (PDB ID 4I4H) was used for comparative
21
22 analysis because this analog is most similar to the investigated compounds.
23
24 Superposition of the **15a**-, **15b**- and GS3-bound structures reveals that **15a** and **15b**
25
26 rotate around the pyridine nitrogen by ca. 180° (Fig. 7C) to place the phenyl/indole rings
27
28 between the heme-ligating pyridine and Arg105 guanidinium group (P2 site), right where
29
30 the Phe-2 side group of GS3 is positioned. Most strikingly, the terminal *Boc* groups are
31
32 in a similar position and displace Phe304 and the I-helix to the same extent as Phe-1 of
33
34 GS3 does (Fig. 7D). Since the phenyl and indole moieties are oriented differently than
35
36 GS3 Phe-2, which is nearly parallel to the pyridine and Arg105 guanidine groups and
37
38 closer to the heme plane, the **15a-b** conformations are less optimal for hydrophobic, π - π
39
40 and π -cation interactions with the heme, pyridine and the Arg105 guanidine,
41
42 respectively. Another important dissimilarity that may decrease affinity of **15a-b** is that
43
44 their binding mode disallows H-bonding with Ser119 (Fig. 7C). Nevertheless, the
45
46 comparable K_s and IC_{50} values for **15b** and GS3 imply that the larger and more electron-
47
48 rich indole ring may partially compensate for the less favorable orientation by
49
50
51
52
53
54
55
56
57
58
59
60

1
2
3 establishing new or more extensive Van der Waals contacts with the neighboring
4
5 Arg105, Ala370, heme and pyridine.
6
7
8
9

11 *Modification of Surface Residues in CYP3A4 for Improvement of Crystal Diffraction –*

12
13 Wild type CYP3A4 willingly co-crystallizes with **4** but, similar to other ligand-bound
14
15 forms, diffraction data of this complex did not exceed 2.5 Å. At this resolution, electron
16
17 density for **4** was discontinuous and the ligand association mode could not be
18
19 accurately determined. To overcome this problem, we decided to introduce surface
20
21 mutations that help form intermolecular contacts in the crystal lattice and improve X-ray
22
23 diffraction power without affecting the CYP3A4 ligand binding and metabolism. Using a
24
25 Surface Entropy Reduction prediction (SERp) server
26
27 (<http://services.mbi.ucla.edu/SER/>),³⁵ several surface peptides containing clusters of
28
29 bulky charged residues (Arg, Lys and/or Glu) were identified (Table 2). One cluster with
30
31 a high score, Lys282/Glu283/Glu285, is part of the surface loop that is disordered in all
32
33 crystal structures reported to date. We mutated this site and found a variant,
34
35 K282A/E285A, that was better expressed in *E. coli*, associated with **4** similarly to the
36
37 wild type, and produced crystals with lower mosaicity and higher diffraction power. This
38
39 mutant was used for determination of the CYP3A4-**4** complex structure.
40
41
42
43
44
45
46
47
48

49 *Crystal Structures of the CYP3A4-4 Complexes –* Co-crystals of CYP3A4 K282A/E285A

50
51 with **4** were grown under two different conditions that led to two distinct modes of ligand
52
53 binding. The first complex was crystallized in the presence of imidazole and contained
54
55 both compound **4** and imidazole in the active site (Fig. 8A). In this structure, determined
56
57
58
59
60

1
2
3 to 1.93 Å, imidazole ligates to the heme iron and **4** binds nearby. Such a ligand
4
5 arrangement is stabilized by two hydrogen bonds formed between the carbonyl oxygen
6
7 and amide nitrogen of **4** and the imidazole nitrogen and the Ser119 hydroxyl group,
8
9 respectively. The pyridine moiety of **4** is adjacent but not embedded into the P1 pocket.
10
11 Through hydrophobic interactions with Phe108, Phe213, Phe215 and Phe340 (Fig. 8B),
12
13 the pyridine ring reinforces the phenylalanine cluster, a unique feature of CYP3A4.³⁶
14
15 The aliphatic linker of **4** forms Van der Waals contacts with the Arg105 side chain,
16
17 whereas the *Boc* group is placed at the P2 site and forms hydrophobic and Van der
18
19 Waals interactions with the Ile369-Ala370 peptide and the Arg212 side chain. Thus,
20
21 when the space near the heme iron is occupied, the flexible compound **4** adopts a
22
23 conformation that allows H-bonding to Ser119 and optimizes hydrophobic interactions
24
25 mediated by the *Boc* and pyridine moieties. It is not clear though why the pyridine of **4**
26
27 does not insert into the P1 pocket as *Boc* of **15a-b** (Fig. 7D) and Phe-2 of GS3 and
28
29 other ritonavir analogs do (Fig. 8C).^{25, 27, 28} The observed orientation may be preferable
30
31 because it prevents steric clashing with Phe304 and the I-helix displacement.
32
33 Alternatively, insertion into the P1 cavity may require some force (*e.g.*, a push), which
34
35 the flexible core of non-ligated **4** cannot provide.
36
37
38
39
40
41
42

43
44 The X-ray structure of the CYP3A4-**4** complex formed in the absence of
45
46 imidazole was determined to 2.25 Å. In this structure, **4** is directly ligated to the heme
47
48 iron *via* the pyridine nitrogen and, similar to **15a-b**, rotates by ~180° relative to GS3
49
50 (Fig. 9). The flexible linker bends to allow the end portion occupy the P2 site. This and
51
52 the lack of H-bonds between **4** and the protein suggest once again that hydrophobic
53
54 interactions, especially at the P2 site, are dominant and define the ligand binding mode.
55
56
57
58
59
60

Conclusions

The data obtained with the first set of rationally designed compounds support the proposed pharmacophore model for a CYP3A4-specific inhibitor and emphasize the importance of pharmacophoric determinants II, III and V (Fig. 3), as well as the dominant role of hydrophobic forces at the P1 and P2 sites during the ligand-binding process. In particular, with this initial set, we were able to confirm that (i) the flexible backbone enables ligands to better fit into the CYP3A4 active site and optimize interactions mediated by the side and terminal moieties; (ii) the P2 site is occupied by ligands first, and interactions at this site are dominant and define the overall ligand binding mode; (iii) the P1 cavity is the second preferable site that ligands tend to occupy, even if it leads to the I-helix distortion; and (iv) H-bonding interactions with Ser119 are established when possible to stabilize the CYP3A4-ligand complex.

There were also new findings that provided additional insights into the ligand binding process. First, pyridine and its short-chain aliphatic derivative, aminoethylpyridine (Fig. 4), were found to be very weak CYP3A4 inactivators (Table 1). This means that ligation of the pyridine nitrogen to the heme iron is weak and dissociable but becomes strong and virtually irreversible when the pyridine ring becomes part of the larger ligands, especially those capable of occupying the P2 and P1 sites. Second, based on the K_s and IC_{50} values for **11**, **15a** and **15b** (Table 1) and the inability of **11** to co-crystallize with CYP3A4, we conclude that aromaticity rather than hydrophobicity of the R_2 substituent is the key feature that stabilizes the protein-ligand complex and drastically improves affinity and inhibitory potency. Third, the

1
2
3 structural data demonstrate that the P1 site can be occupied by the terminal group if R₁
4 is absent. That none of the R₁-lacking compounds markedly affected CYP3A4 T_m
5 suggests, however, that *Boc*-mediated interactions at the P1 site are sub-optimal and
6 cannot provide the binding energy on the same scale as phenyl substituents of R₁ do
7 (e.g., in ritonavir and GS3). Fourth, there was no correlation between ΔT_m and IC₅₀ for
8 the investigated compounds (Table 1) but, as observed for other ritonavir analogs,^{27, 28}
9 the inhibitory potency was proportional to the 442 nm absorption of the ferrous ligand-
10 bound species. Thus, during ligand screening, the latter parameter may predict strong
11 CYP3A4 inactivators more reliably than ΔT_m . Finally, two of the rationally designed
12 compounds, **15a** and **15b**, are less structurally complex than GS3 and ritonavir but
13 inhibit CYP3A4 with a comparable, sub-micromolar potency. This raises the possibility
14 that simpler and more potent CYP3A4 inactivators than ritonavir can be designed
15 through **15a-b** optimization.
16
17
18
19
20
21
22
23
24
25
26
27
28
29
30
31
32
33
34
35
36

37 Experimental Procedures

38 *Synthesis of analogs*

39
40
41 **Synthesis of compound 2.** Di-*tert*-butyloxycarbonyl, (Boc)₂O (1.99g, 9.14mmol) was added
42 to a solution of 6-aminohexanoic acid (1g, 7.61mmol) and NaOH (10% aqueous solution) in
43 1,4-dioxane. The reaction mixture was then stirred overnight at room temperature. The
44 solvent was evaporated and the mixture was acidified using 1N HCl. The acidified mixture
45 was then extracted with dichloromethane (DCM). The organic layer was washed with brine,
46 dried over Na₂SO₄, filtered and concentrated. The crude material was then purified using
47 column chromatography to give the pure product **2** (1.57g, 89%).
48
49
50
51
52
53
54
55
56
57
58
59
60

Synthesis of compounds 4 and 5 (Scheme 1). Compound **2** (1g, 4.23mmol) was added to a solution of EDAC (1.67g, 10.80mmol) in dimethylformamide (DMF). The mixture was stirred at room temperature for 30 min after which DIPEA (3.76 mL, 21.61mmol) and 3-(aminomethyl)pyridine, **3** (0.70g, 6.34mmol) were added to the reaction mixture. The reaction was allowed to stir for 16 h. On completion, the solvent was evaporated and the reaction mixture was diluted with ethylacetate. The organic layer was then washed with saturated NaHCO₃, water and brine. The combined organic layer was dried over Na₂SO₄ and concentrated to give the crude product which was then purified using column chromatography (ethylacetate:methanol). The pure product **4** was obtained as white solid in 65% yield (0.91g). ¹H NMR (CDCl₃, 500 MHz) δ 8.53 (s, 2H), 7.64 (d, *J* = 7.82 Hz, 1H), 7.27 (t, *J* = 4.80 Hz, 1H), 5.95 (bs, 1H), 4.56 (bs, 1H), 4.46 (d, *J* = 5.91 Hz, 2H), 3.10 (q, *J* = 6.45 Hz, 2H), 2.23 (t, *J* = 7.45 Hz, 2H), 1.68 (quin, *J* = 7.5 Hz, 2H), 1.50-1.46 (m, 2H), 1.42 (s, 9H), 1.34 (m, 2H); ¹³C NMR (CDCl₃, 125 MHz) δ 149.1, 148.8, 135.8, 123.7, 41.0, 36.4, 29.8, 28.4, 26.3, 25.2; HRMS *m/z* calculated for C₁₇H₂₇N₃O₃ [M+Na]⁺: 344.21, found: 344.2.

Compound **4** (0.6g, 1.86mmol) was treated with trifluoroacetic acid in DCM for 14 h at room temperature in order to remove the *Boc*-group. The completion of the reaction was monitored through TLC. The reaction solvent was evaporated and the crude product was passed through celite to obtain the pure amine **5** (0.47g, 78yield%). ¹H-NMR (500 MHz, CD₃OD) δ 8.81 (1H, s), 8.79-8.78 (2H, d, *J* = 5.5 Hz), 8.53-8.51 (1H, d, *J* = 8.3 Hz), 8.06-8.03 (1H, m), 2.97-2.91 (2H, m), 2.37-2.34 (2H, t, *J* = 7.4 Hz), 1.72-1.68 (4H, m), 1.48-1.39 (4H, m); ¹³C NMR (CD₃OD, 125 MHz) δ 175.2, 161.1, 144.5, 142.4, 139.2, 126.4, 39.7, 38.9, 34.3, 29.8, 26.6, 24.3. HRMS *m/z* calculated for C₁₂H₁₉N₃O [M+H]⁺: 222.23, found: 222.2.

1
2
3
4
5
6 After optimizing different conditions and routes, we started synthesis of the first generation
7
8 analogs using (*S*)-*Boc*-phenylalaninol as shown in Schemes 2 and 3. (*S*)-*Boc*-phenylalaninol
9
10 or other corresponding amino alcohols (shown in the schemes) were converted to a tosylate
11
12 using *p*-toluenesulphonyl chloride, which was then reacted with 3-mercaptopropionic acid in
13
14 the presence of NaOH at 50°C to give the corresponding acid. The acid was then coupled to
15
16 the 2-(3-pyridyl)ethylamine using the known usual EDAC coupling to give the corresponding
17
18 final product.
19
20
21
22
23

24
25 **Synthesis of compound 7.** *S*-*Boc*-phenylalaninol (2g, 7.96mmol) was dissolved in
26
27 methanol and treated with rhodium on charcoal (5%; 100mg) under H₂ atmosphere
28
29 overnight to reduce the phenyl ring. The solution was then passed through celite plug, and
30
31 methanol was evaporated to give the pure product **7** in quantitative yield (2.01g, quant).
32
33
34
35

36
37 **Synthesis of compound 8.** *S*-*Boc*-cyclohexylalaninol (2g, 7.78mmol) was dissolved in
38
39 DCM. To this solution, triethylamine (3.25mL, 23.34mmol) and *p*-toluenesulphonyl chloride
40
41 (2.23g, 11.67mmol) were added slowly at 0°C. The reaction was then allowed to stir at room
42
43 temperature overnight. After reaction completion, DCM was evaporated and the crude
44
45 reaction mixture was purified using column chromatography. The pure product **8** was
46
47 obtained as white fluffy solid (2.3g, 71% yield). LCMS *m/z* calculated for C₂₁H₃₃NO₅S
48
49 [M+Na]⁺: 434.21, found 434.23.
50
51
52
53
54
55
56
57
58
59
60

Synthesis of compound 10. To solution of compound **8** (1g, 2.43mmol) in DMF, 3-mercaptopropanoic acid, **9** (0.309g, 2.91mmol) was added. To this mixture, 1N NaOH (2 mL) was added and reaction was allowed to stir for 5 h at 50°C. The crude product **10** was obtained by evaporating the solvent and was used for the next step without any further purification due to instability of the product on silica column. LCMS m/z calculated for C₁₇H₃₁NO₄S [M+2Na]⁺: 368.20, found 368.17.

Synthesis of compound 11. Compound **10** (0.1g, 0.3mmol) was added to a solution of EDAC (0.12g, 0.72mmol) in DMF. The mixture was stirred at room temperature for 30 min after which DIPEA (0.23mL, 1.45mmol) and 3-(aminomethyl)pyridine, **3** (0.042g, 0.43mmol) were added. The reaction was allowed to stir for 18 h. On completion, the solvent was evaporated and the reaction mixture was diluted with ethylacetate. The organic layer was then washed with saturated NaHCO₃, water and brine. The combined organic layers were dried over Na₂SO₄ and concentrated to give the crude product which was then purified using column chromatography (ethylacetate:methanol). The pure product **11** was obtained as yellow oil in 22% yield (0.005g). ¹H-NMR (400 MHz, CD₂Cl₂) δ 9.31-9.07 (1H, m), 8.56 (2H, bs), 7.70-7.57 (2H, m), 7.33 (1H, bs), 4.54 (1H, s), 3.74-3.20 (5H, m), 3.14-3.04 (6H, m), 2.43-2.26 (1H, m), 1.67-1.51 (4H, m), 1.44-1.33 (2H, m), 1.26 (8H, s), 1.17-1.11 (3H, m), 1.04 (3H, m). ¹³C NMR (100 MHz, CD₂Cl₂) δ 132.6, 130.5, 64.4, 32.0, 31.6, 29.9, 29.3, 27.0, 24.7, 23.4, 22.9, 22.5, 15.4, 15.2, 14.6, 13.8, 12.8, 12.0. LCMS m/z calculated for C₂₃H₃₇N₃O₃S [M+Na]⁺: 458.22, found 458.21.

General procedure for synthesis of compounds 15a and 15b

Synthesis of compound 13a. *S*-Boc-phenylalaninol (1g, 3.98mmol) was dissolved in DCM. To this solution, triethylamine and *p*-toluenesulphonyl chloride were added slowly at 0°C. The reaction was then allowed to stir at room temperature overnight. After reaction completion, DCM was evaporated and the crude reaction mixture was purified using column chromatography. The pure product **13a** was obtained as white fluffy solid in 78% yield (1.26g). The pure product **13b** was obtained as white solid in 81% yield.

Synthesis of compound 14a. To the solution of compound **13a** (0.5g, 1.23mmol) in DMF, 3-mercaptopropanoic acid, **9** (0.157g, 1.48mmol) was added. To this mixture, 1N NaOH (2 mL) was added and reaction was allowed to stir at 50°C for 5 h. The crude product **14a** was obtained by evaporating the solvent and was used for the next step without any further purification. LCMS *m/z* calculated for **14a**: C₁₇H₂₅NO₄S [M+Na]⁺: 362.15, found 362.17. LCMS *m/z* calculated for **14b**: C₁₉H₂₆N₂O₄S [M-H]⁺: 378.20, found 377.14.

Synthesis of compound 15a. Compound **14a** (0.5g, 1.47mmol) was added to a solution of EDAC (0.57g, 3.67mmol) in DMF. The mixture was stirred at room temperature for 30 min after which DIPEA (1.28mL, 7.35mmol) and 3-(aminomethyl)pyridine, **3** (0.24g, 2.21mmol) were added. The reaction was allowed to stir for 18 h. On completion, the solvent was evaporated and the reaction mixture was diluted with ethylacetate. The organic layer was then washed with saturated NaHCO₃, water and brine. The combined organic layers were dried over Na₂SO₄ and concentrated to give the crude product which was then purified using column chromatography (ethylacetate:methanol). The pure product **15a** was obtained as white solid in 62% yield (0.39g). ¹H NMR (CDCl₃, 500 MHz) δ 8.54 (d, *J* = 14.4 Hz, 2H), 7.66

Kaur et al. *Evaluation of the CYP3A4 inhibitor pharmacophore model*

18

(d, $J = 9.4$ Hz, 1H), 7.31-7.16 (m, 6H), 6.69 (bs, 1H), 4.72 (d, $J = 10.3$ Hz, 1H), 4.52-4.40 (m, 2H), 2.87 (t, $J = 9.3$ Hz, 3H), 2.63-2.51 (m, 4H), 1.40 (d, $J = 4.15$ Hz, 2H), 1.36 (s, 9H); ^{13}C NMR (CDCl_3 , 125 MHz) δ 149.2, 148.8, 135.6, 129.4, 129.3, 128.8, 128.6, 126.7, 123.6, 41.0, 36.6, 28.6, 28.3; HRMS m/z calculated for $\text{C}_{23}\text{H}_{31}\text{N}_3\text{O}_3\text{S}$ $[\text{M}+\text{H}]^+$: 430.231, found 430.21.

The pure product **15b** was obtained as yellow oil in 56% yield. ^1H NMR (CDCl_3 , 500 MHz) δ 8.51 (bs, 2H), 8.25 (s, 1H), 7.64 (d, $J = 7.59$ Hz, 2H), 7.35 (d, $J = 8.07$ Hz, 1H), 5.95 (bs, 1H), 7.23 (t, $J = 4.85$ Hz, 1H), 7.18 (t, $J = 7.58$ Hz, 1H), 7.11 (t, $J = 7.28$ Hz, 1H), 7.02 (s, 1H), 6.54 (s, 1H), 4.76 (bs, 1H), 4.41 (t, $J = 5.91$ Hz, 2H), 4.05 (m, 1H), 3.01 (bs, 2H), 2.86 (bm, 2H), 2.62 (bm, 2H), 2.49 (bm, 2H), 1.36 (s, 9H); ^{13}C NMR (CDCl_3 , 125 MHz) δ 155.7, 149.1, 148.7, 136.3, 135.7, 134.1, 129.4, 126.6, 123.6, 122.9, 122.2, 119.7, 119.0, 111.3, 111.2, 50.7, 41.0, 36.5, 35.8, 28.8, 28.4.; HRMS m/z calculated for $\text{C}_{17}\text{H}_{27}\text{N}_3\text{O}_3$ $[\text{M}+\text{Na}]^+$: 491.21, found 491.2.

The purity of compounds **4**, **5**, **15a** and **15b** was >95% as determined by ^1H NMR analysis. The purity of compound **11**, however, did not exceed 90% even after repeated attempts of column chromatography purification.

Protein Expression and Purification – The K282A/E285A mutation was introduced to the CYP3A4 Δ 3-22 expression plasmid using a QuikChange mutagenesis kit (Stratagene). The C-terminally 4-histidine tagged wild type and mutant CYP3A4 were produced, purified and quantified as reported previously.²⁵

1
2
3 *Spectral Binding Titrations* - Ligand binding to CYP3A4 was monitored in 50 mM
4 phosphate, pH 7.4, containing 20% glycerol and 1 mM dithiothreitol (buffer A) in a Cary
5 300 spectrophotometer. The protein was titrated with small aliquots of the investigated
6 compounds dissolved in dimethyl sulfoxide, with the final solvent concentration <2%.
7
8 Spectral dissociation constants (K_s) were determined from the titration curves using
9 one- or two-site saturation fitting.
10
11
12
13
14
15
16
17
18
19

20 *Kinetics of Ligand Binding* - Kinetics of ligand binding to CYP3A4 was monitored at
21 room temperature in 50 mM phosphate, pH 7.4, in a SX.18MV stopped flow apparatus
22 (Applied Photophysics, UK) after mixing 2 μ M CYP3A4 with various concentrations of
23 ligands. Absorbance changes were followed at 409-411 nm for pyridine,
24 aminoethylpyridine and compound **5**, and at 427-428 nm for **4**, **11**, and **15a-b**. Kinetic
25 data were analyzed using the program IgorPro (WaveMetrics, Inc).
26
27
28
29
30
31
32
33
34
35

36 *Thermal Denaturation and Inhibitory Potency Assays* – Thermal denaturation
37 experiments were conducted as previously described²⁷ to compare ligand-dependent
38 changes in CYP3A4 stability. The inhibitory potency of the investigated compounds on
39 the 7-benzyloxy-4-(trifluoromethyl)coumarin (BFC) O-debenzylation activity of CYP3A4
40 was evaluated fluorometrically in a reconstituted system with rat cytochrome P450
41 reductase (CPR). The reaction was carried out at room temperature in 100 mM
42 phosphate buffer, pH 7.4, containing catalase and superoxide dismutase (2 Units/ml
43 each). A mixture of 1 μ M CYP3A4 and 1 μ M CPR was preincubated for 1 hour at room
44 temperature and diluted by 20-fold with the assay buffer immediately before
45
46
47
48
49
50
51
52
53
54
55
56
57
58
59
60

1
2
3 measurements. BFC (50 μ M) and various concentrations of analogs were added to the
4
5 protein mixture 2 minutes prior to the reaction initiation with 100 μ M NADPH. Formation
6
7 of 7-hydroxy-4-trifluoromethylcoumarin was followed in a Hitachi F100 fluorometer using
8
9 $\lambda_{\text{ex}} = 430$ nm and $\lambda_{\text{em}} = 500$ nm. IC_{50} values were derived from the [% activity] vs.
10
11 [inhibitor] plots.
12
13
14
15
16
17

18 *Crystallization and Determination of the X-ray Structures of Ligand-bound CYP3A4 -*
19
20 CYP3A4 K282A/E285A was co-crystallized with **4** by a sitting drop vapor diffusion
21
22 method. Protein (80 mg/ml) in buffer A was mixed with a 10-fold excess of **4** and
23
24 centrifuged to remove the precipitate. CYP3A4 K282A/E285A directly ligated to **4** was
25
26 crystallized against the 80% solution E7 from the Morpheus crystallization screen
27
28 (Molecular Dimensions). The imidazole-containing solution A3 from the same screening
29
30 kit resulted in co-crystallization of the mutant with both imidazole and **4** in the active site.
31
32
33 Crystals of the wild type CYP3A4 bound to compounds **15a** and **15b** were grown by a
34
35 microbatch method under oil. A half of a microliter of ligand-bound CYP3A4 was mixed
36
37 with 0.5 μ l of 6-10% polyethylene glycol 3,350 and 60-90 mM sodium malonate, pH 5.0,
38
39 and covered with paraffin oil. All crystals were cryoprotected with Paratone-N and
40
41 frozen in liquid nitrogen. X-ray diffraction data were collected at the Stanford
42
43 Synchrotron Radiation Lightsource beamline 7-1 and the Advanced Light Source
44
45 beamline 8.2.1. Crystal structures were solved by molecular replacement with
46
47 PHASER³⁷ and the ligand-free 1TQN structure as a search model. The initial models
48
49 were rebuilt and refined with COOT³⁸, PHENIX³⁹ and REFMAC.³⁷ Data collection and
50
51 refinement statistics are summarized in the Supporting Information Table 1S. The
52
53
54
55
56
57
58
59
60

1
2
3 atomic coordinates and structure factors for **4**-, imidazole/**4**-, **15a**- and **15b**-bound
4
5 CYP3A4 have been deposited in the Protein Data Bank with the ID codes 4D75, 4D6Z,
6
7 4D78 and 4D7D, respectively.
8
9

10 11 12 **Supporting Information**

13
14
15 The X-ray data collection and refinement statistics, and mass spectrometry and NMR
16
17 data for compounds **4-15a/b**. This material is available free of charge via the Internet at
18
19 <http://pubd.acs.org>.
20
21

22
23
24 **PDB ID codes:** 4D75, 4D6Z, 4D78 and 4D7D.
25
26

27 28 29 **Author Information**

30
31
32 Corresponding Author:

33
34 *Email: sevrioui@uci.edu. Phone: (949) 824-1953.
35
36

37 38 39 **Present address**

40
41 §William Paterson University, 300 Pompton Road, Wayne NJ 07470.
42
43

44 45 46 **Notes**

47
48 The authors declare no competing financial interest.
49
50

51 52 53 **Acknowledgement**

54
55
56 This work was supported by the N.I.H. National Institute of General Medical Sciences
57
58
59
60

(GM57353, T.L.P.) and the University of California's Center for Antiviral Drug Discovery (MRPI 143226, A.R.C.), and involves research carried out at the Advanced Light Source and the Stanford Synchrotron Radiation Lightsource, a national user facility operated by Stanford University on behalf of the U.S. Department of Energy, Office of Basic Energy Sciences. The Advanced Light Source is supported by the Director, Office of Science, Office of Basic Energy Sciences, of the U.S. Department of Energy under Contract No. DE-AC0205CH11231. The SSRL Structural Molecular Biology Program is supported by the Department of Energy, Office of Biological and Environmental Research, and by National Institutes of Health, National Center for Research Resources, Biomedical and Technology Program, and the National Institute of General Medical Sciences. The authors also thank J. Milligan and M. Vasquez for technical assistance.

Abbreviations

CYP3A4, 3A4 isoform of cytochrome P450; CPR, cytochrome P450 reductase; BFC, 7-benzyloxy-4-(trifluoromethyl)coumarin.

References

- (1) Guengerich, F. P.; Shimada, T. Oxidation of toxic and carcinogenic chemicals by human cytochrome P-450 enzymes. *Chem. Res. Toxicol.* **1991**, 4, 391-407.
- (2) Li, A. P.; Kaminski, D. L.; Rasmussen, A. Substrates of human hepatic cytochrome P450 3A4. *Toxicology* **1995**, 104, 1-8.
- (3) Guengerich, F. P. Cytochrome P-450 3A4: regulation and role in drug metabolism. *Annu. Rev. Pharmacol. Toxicol.* **1999**, 39, 1-17.

(4) Mehmood, Z.; Kelly, D. E.; Kelly, S. L. Cytochrome P450 3A4 mediated metabolism of 2,4-dichlorophenol. *Chemosphere* **1997**, 34, 2281-2291.

(5) Chae, Y. H.; Yun, C. H.; Guengerich, F. P.; Kadlubar, F. F.; el-Bayoumy, K. Roles of human hepatic and pulmonary cytochrome P450 enzymes in the metabolism of the environmental carcinogen 6-nitrochrysene. *Cancer. Res.* **1993**, 53, 2028-2034.

(6) Hodgson, E. In vitro human phase I metabolism of xenobiotics I: pesticides and related compounds used in agriculture and public health. *J. Biochem. Mol. Toxicol.* **2003**, 17, 201-206.

(7) Mehmood, Z.; Williamson, M. P.; Kelly, D. E.; Kelly, S. L. Human cytochrome P450 3A4 is involved in the biotransformation of the herbicide 2,4-dichlorophenoxyacetic acid. *Environ. Toxicol. Pharmacol.* **1996**, 2, 397-401.

(8) Mehmood, Z.; Williamson, M. P.; Kelly, D. E.; Kelly, S. L. Metabolism of organochlorine pesticides: the role of human cytochrome P450 3A4. *Chemosphere* **1996**, 33, 759-769.

(9) Kempf, D. J.; Marsh, K. C.; Kumar, G.; Rodrigues, A. D.; Denissen, J. F.; McDonald, E.; Kukulka, M. J.; Hsu, A.; Granneman, G. R.; Baroldi, P. A.; Sun, E.; Pizzuti, D.; Plattner, J. J.; Norbeck, D. W.; Leonard, J. M. Pharmacokinetic enhancement of inhibitors of the human immunodeficiency virus protease by coadministration with ritonavir. *Antimicrob. Agents Chemother.* **1997**, 41, 654-660.

(10) Xu, L.; Desai, M. C. Pharmacokinetic enhancers for HIV drugs. *Curr. Opin. Investig. Drugs.* **2009**, 10, 775-786.

(11) Mathias, A. A.; German, P.; Murray, B. P.; Wei, L.; Jain, A.; West, S.; Warren, D.; Hui, J.; Kearney, B. P. Pharmacokinetics and pharmacodynamics of GS-9350: a novel

1
2
3 pharmacokinetic enhancer without anti-HIV activity. *Clin. Pharmacol. Ther.* **2010**, *87*,
4
5 322-329.

6
7
8 (12) Xu, L.; Liu, H.; Murray, B.; Callebaut, C.; Lee, M. S.; Hong, A.; Strickley, R. G.;
9
10 Tsai, L. K. ; Stray, K. M.; Wang, Y.; Rhodes, G. R.; Desai, M. C. Cobicistat (GS-9350):
11
12 A potent and selective inhibitor of human CYP3A as a novel pharmacoenhancer. *ACS*
13
14 *Med. Chem. Lett.* **2010**, *1*, 209-213.

15
16
17 (13) Xu, L.; Liu, H.; Hong, A.; Vivian, R.; Murray, B. P.; Callebaut, C.; Choi, Y. C.; Lee,
18
19 M. S.; Chau, J.; Tsai, L. K.; Stray, K. M.; Strickley, R. G.; Wang, J.; Tong, L.;
20
21 Swaminathan, S.; Rhodes, G. R.; Desai, M. C. Structure-activity relationships of
22
23 diamine inhibitors of cytochrome P450 (CYP) 3A as novel pharmacoenhancers. Part II:
24
25 P2/P3 region and discovery of cobicistat (GS-9350). *Bioorg. Med. Chem. Lett.* **2014**, *24*,
26
27 995-999.

28
29
30 (14) Kempf, D. J.; Marsh, K. C.; Denissen, J. F.; McDonald, E.; Vasavanonda, S.;
31
32 Flentge, C. A.; Green, B. E.; Fino, L.; Park, C. H.; Kong, X. P.; et al. ABT-538 is a potent
33
34 inhibitor of human immunodeficiency virus protease and has high oral bioavailability in
35
36 humans. *Proc. Natl. Acad. Sci. U S A* **1995**, *92*, 2484-2488.

37
38
39 (15) Koudriakova, T.; Iatsimirskaia, E.; Utkin, I.; Gangl, E.; Vouros, P.; Storozhuk, E.;
40
41 Orza, D.; Marinina, J.; Gerber, N. Metabolism of the human immunodeficiency virus
42
43 protease inhibitors indinavir and ritonavir by human intestinal microsomes and
44
45 expressed cytochrome P4503A4/3A5: mechanism-based inactivation of cytochrome
46
47 P4503A by ritonavir. *Drug Metab. Dispos.* **1998**, *26*, 552-561.
48
49
50
51
52
53
54
55
56
57
58
59
60

(16) von Moltke, L. L.; Durol, A. L.; Duan, S. X.; Greenblatt, D. J. Potent mechanism-based inhibition of human CYP3A in vitro by amprenavir and ritonavir: comparison with ketoconazole. *Eur. J. Clin. Pharmacol.* **2000**, *56*, 259-261.

(17) Ernest, C. S., 2nd; Hall, S. D.; Jones, D. R. Mechanism-based inactivation of CYP3A by HIV protease inhibitors. *J. Pharmacol. Exp. Ther.* **2005**, *312*, 583-591.

(18) Lin, H. L.; D'Agostino, J.; Kanaan, C.; Calinski, D.; Hollenberg, P. F. The effect of ritonavir on human CYP2B6 catalytic activity: heme modification contributes to the mechanism-based inactivation of CYP2B6 and CYP3A4 by ritonavir. *Drug Metab. Dispos.* **2013**, *41*, 1813-1824.

(19) Rock, B. M.; Hengel, S. M.; Rock, D. A.; Wienkers, L. C.; Kunze, K. L. Characterization of Ritonavir-Mediated Inactivation of Cytochrome P450 3A4. *Mol. Pharmacol.* **2014**, *86*, 665-674.

(20) Sekiguchi, N.; Higashida, A.; Kato, M.; Nabuchi, Y.; Mitsui, T.; Takanashi, K.; Aso, Y.; Ishigai, M. Prediction of drug-drug interactions based on time-dependent inhibition from high throughput screening of cytochrome P450 3A4 inhibition. *Drug Metab. Pharmacokinet.* **2009**, *24*, 500-510.

(21) Iribarne, C.; Berthou, F.; Carlhant, D.; Dreano, Y.; Picart, D.; Lohezic, F.; Riche, C. Inhibition of methadone and buprenorphine N-dealkylations by three HIV-1 protease inhibitors. *Drug Metab. Dispos.* **1998**, *26*, 257-260.

(22) Eagling, V. A.; Back, D. J.; Barry, M. G. Differential inhibition of cytochrome P450 isoforms by the protease inhibitors, ritonavir, saquinavir and indinavir. *Br. J. Clin. Pharmacol.* **1997**, *44*, 190-194.

- 1
2
3
4
5
6
7
8
9
10
11
12
13
14
15
16
17
18
19
20
21
22
23
24
25
26
27
28
29
30
31
32
33
34
35
36
37
38
39
40
41
42
43
44
45
46
47
48
49
50
51
52
53
54
55
56
57
58
59
60
- (23) Kumar, G. N.; Rodrigues, A. D.; Buko, A. M.; Denissen, J. F. Cytochrome P450-mediated metabolism of the HIV-1 protease inhibitor ritonavir (ABT-538) in human liver microsomes. *J. Pharmacol. Exp. Ther.* **1996**, *277*, 423-431.
- (24) Zalma, A.; von Moltke, L. L.; Granda, B. W.; Harmatz, J. S.; Shader, R. I.; Greenblatt, D. J. In vitro metabolism of trazodone by CYP3A: inhibition by ketoconazole and human immunodeficiency viral protease inhibitors. *Biol. Psychiatry* **2000**, *47*, 655-661.
- (25) Sevrioukova, I. F.; Poulos, T. L. Structure and mechanism of the complex between cytochrome P4503A4 and ritonavir. *Proc. Natl. Acad. Sci. U S A* **2010**, *107*, 18422-18427.
- (26) Sevrioukova, I. F.; Poulos, T. L. Interaction of human cytochrome P4503A4 with ritonavir analogs. *Arch. Biochem. Biophys.* **2012**, *520*, 108-116.
- (27) Sevrioukova, I. F.; Poulos, T. L. Pyridine-substituted desoxyritonavir is a more potent cytochrome P450 3A4 inhibitor than ritonavir. *J. Med. Chem.* **2013**, *56*, 3733-3741.
- (28) Sevrioukova, I. F.; Poulos, T. L. Dissecting cytochrome P450 3A4-ligand interactions using ritonavir analogues. *Biochemistry* **2013**, *52*, 4474-4481.
- (29) Sevrioukova, I. F.; Poulos, T. L. Ritonavir analogues as a probe for deciphering the cytochrome P450 3A4 inhibitory mechanism. *Curr. Top. Med. Chem.* **2014**, *14*, 1348-1355.
- (30) Ekins, S.; Bravi, G.; Binkley, S.; Gillespie, J. S.; Ring, B. J.; Wikel, J. H.; Wrighton, S. A. Three- and four-dimensional quantitative structure activity relationship

1
2
3 analyses of cytochrome P-450 3A4 inhibitors. *J. Pharmacol. Exp. Ther.* **1999**, 290, 429-
4
5 438.

6
7
8 (31) Ekins, S.; Bravi, G.; Wikel, J. H.; Wrighton, S. A. Three-dimensional-quantitative
9
10 structure activity relationship analysis of cytochrome P-450 3A4 substrates. *J.*
11
12 *Pharmacol. Exp. Ther.* **1999**, 291, 424-433.

13
14
15 (32) Ekins, S.; Stresser, D. M.; Williams, J. A. In vitro and pharmacophore insights
16
17 into CYP3A enzymes. *Trends Pharmacol. Sci.* **2003**, 24, 161-166.

18
19
20 (33) Riley, R. J.; Parker, A. J.; Trigg, S.; Manners, C. N. Development of a
21
22 generalized, quantitative physicochemical model of CYP3A4 inhibition for use in early
23
24 drug discovery. *Pharm. Res.* **2001**, 18, 652-655.

25
26
27 (34) Liu, H.; Xu, L.; Hui, H.; Vivian, R.; Callebaut, C.; Murray, B. P.; Hong, A.; Lee, M.
28
29 S.; Tsai, L. K.; Chau, J. K.; Stray, K. M.; Cannizzaro, C.; Choi, Y. C.; Rhodes, G. R.;
30
31 Desai, M. C. Structure-activity relationships of diamine inhibitors of cytochrome P450
32
33 (CYP) 3A as novel pharmacoenhancers, part I: core region. *Bioorg. Med. Chem. Lett.*
34
35 **2014**, 24, 989-994.

36
37
38 (35) Goldschmidt, L.; Cooper, D. R.; Derewenda, Z. S.; Eisenberg, D. Toward rational
39
40 protein crystallization: A Web server for the design of crystallizable protein variants.
41
42 *Protein Sci.* **2007**, 16, 1569-1576.

43
44
45 (36) Williams, P. A.; Cosme, J.; Vinkovic, D. M.; Ward, A.; Angove, H. C.; Day, P. J.;
46
47 Vonrhein, C.; Tickle, I. J.; Jhoti, H. Crystal structures of human cytochrome P450 3A4
48
49 bound to metyrapone and progesterone. *Science* **2004**, 305, 683-686.

50
51
52 (37) CCP4. Collaborative computational project number 4. The CCP4 suite programs
53
54 for protein crystallography. *Acta Crystallogr. Section D* **1994**, 50, 760-763.
55
56
57
58
59
60

1
2
3 (38) Emsley, P.; Lohkamp, B.; Scott, W. G.; Cowtan, K. Features and development of
4
5 Coot. *Acta Crystallogr. Section D* **2010**, 66, 486-501.
6
7

8 (39) Adams, P. D.; Afonine, P. V.; Bunkoczi, G.; Chen, V. B.; Davis, I. W.; Echols, N.;
9
10 Headd, J. J.; Hung, L. W.; Kapral, G. J.; Grosse-Kunstleve, R. W.; McCoy, A. J.;
11
12 Moriarty, N. W.; Oeffner, R.; Read, R. J.; Richardson, D. C.; Richardson, J. S.;
13
14 Terwilliger, T. C.; Zwart, P. H. PHENIX: a comprehensive Python-based system for
15
16 macromolecular structure solution. *Acta Crystallogr Section D* **2010**, 66, 213-221.
17
18
19
20
21
22
23
24
25
26
27
28
29
30
31
32
33
34
35
36
37
38
39
40
41
42
43
44
45
46
47
48
49
50
51
52
53
54
55
56
57
58
59
60

Table 1. Properties of pyridine-containing compounds

	442 nm band ^a (Fe ²⁺)	K _s ^b (μM)	k _{fast} ^c (s ⁻¹)	ΔT _m ^d (°C)	IC ₅₀ ^e (μM)
pyridine	-	4500±400	0.5±0.1	0	4000±500
aminoethylpyridine	-	2500±200	0.6±0.1	-0.1	5000±600
5	-	10±1 ^f 4400±500 ^f	0.8±0.1	-0.2	1000±150
4	+	105±10	20±2	-0.2	75±5
11	+	10±1	4.0±0.2	-2±0.4	30±3
15a	++	0.9±0.1	1.7±0.2	-1±0.2	0.52±0.05
15b	++	0.5±0.1	8.0±1.5	0.2	0.21±0.04
GS3 ^g	+++	0.025	7.0	5.1	0.13
ritonavir ^g	+++	0.051	1.4	2.7	0.55

^a Appearance and magnitude of the 442 nm peak in the absorbance spectrum of ligand-bound ferrous CYP3A4.

^b Spectral dissociation constant.

^c Rate constant for the fast phase of the binding reaction measured at saturating ligand concentrations.

^d Ligand-dependent changes in the melting temperature of CYP3A4.

^e Concentration required for half-maximal inactivation of recombinant CYP3A4.

^f Values derived from the two site saturation fit to a titration curve.

^g Determined previously.^{25, 27}

Table 2. High entropy residues in CYP3A4 identified by a Surface Entropy Reduction prediction (SERp) server (<http://services.mbi.ucla.edu/SER/>).³⁵

Cluster	Residues	SERp score ^a	Proposed mutations
1	⁴²¹ KKNK ⁴²⁴	6.51	K421A/K422A/K424A
2	²⁸² KETESHKA ²⁸⁹	6.3	K282A/E263A/E285A
3	⁴⁶⁹ KETQ ⁴⁷²	5.26	K469A/E470A
4	⁴⁸⁶ EK ⁴⁸⁷	5.09	E486A/K487A
5	³⁷⁸ KKDVE ³⁸²	5.07	K378A/K379A

^a The highest score is assigned to a cluster with the highest probability to enhance crystallizability upon mutation.

Figure Legends

Figure 1. Chemical structures of ritonavir, cobicistat and GS3. The phenyl side groups proximal and distant from the heme-ligating moiety are designated as Phe-1 and Phe-2, respectively.

Figure 2. Pharmacophore model for a CYP3A4-specific inhibitor derived from the structure/function studies on analogues of ritonavir. Pharmacophoric determinants: I – strong heme-ligating nitrogen donor, II - flexible backbone, III and IV – aromatic and hydrophobic moieties, respectively, V - hydrogen donor/acceptor, IV - poly-functional end-group. The P1 and P2 sites are hydrophobic pockets adjacent to the phenylalanine cluster and the heme, respectively.

Figure 3. A scaffold used for the CYP3A4 inhibitor design. The pyridine ring, serving as a heme-ligating moiety, is attached to a flexible backbone *via* a peptide bond, an H-donor/acceptor. By varying the side (R_1 and R_2) and terminal (R_3) groups, the role of each moiety in the CYP3A4 binding and inhibition can be probed.

Figure 4. Chemical structures of the investigated compounds.

Figure 5. A-C, Spectral changes induced in CYP3A4 by pyridine, aminoethylpyridine and compound **5**, respectively. Absorbance spectra of the ferric ligand-free, ligand-bound and ferrous ligand-bound forms are shown in solid, dashed and dotted lines, respectively. Insets (a) are absorbance changes observed during equilibrium titration of

1
2
3
4
5
6
7
8
9
10
11
12
13
14
15
16
17
18
19
20
21
22
23
24
25
26
27
28
29
30
31
32
33
34
35
36
37
38
39
40
41
42
43
44
45
46
47
48
49
50
51
52
53
54
55
56
57
58
59
60

CYP3A4 with pyridine, aminoethylpyridine and **5**. Insets (*b*) are plots of absorbance change vs. ligand concentration.

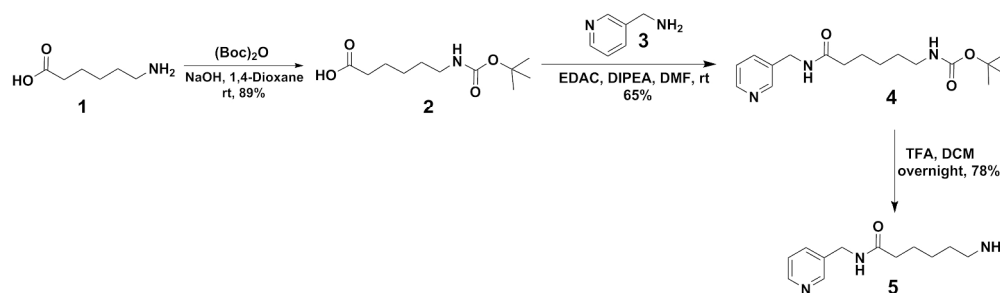
Figure 6. *A-D*, Spectral changes induced in CYP3A4 by compounds **4**, **11**, **15a** and **15b**, respectively. Absorbance spectra of the ferric ligand-free, ligand-bound and ferrous ligand-bound forms are shown in solid, dashed and dotted lines, respectively. Absorbance maxima of the ferric and ferrous ligand-bound CYP3A4 are indicated. Insets (*a*) are absorbance changes observed during equilibrium titration of CYP3A4 with **4**, **11** and **15a-b**. Insets (*b*) are plots of absorbance change vs. ligand concentration.

Figure 7. *A* and *B*, The active site of CYP3A4 bound to compounds **15a** and **15b**, respectively. The ligands (in green), heme (in pink) and the Arg105 side group are shown in stick representation. $2F_o-F_c$ electron density maps are contoured at 1σ . *C* and *D*, Relative orientation of **15a** (green), **15b** (light gray) and GS3 (magenta). Panel *C* shows that a 180° rotation of **15a** and **15b** relative to GS3 prevents H-bond formation with Ser119. Panel *D* demonstrates that the *Boc* groups of **15a** and **15b** occupy the P1 site and displace the I-helix Phe304 to the same extent as GS3 Phe-1 does.

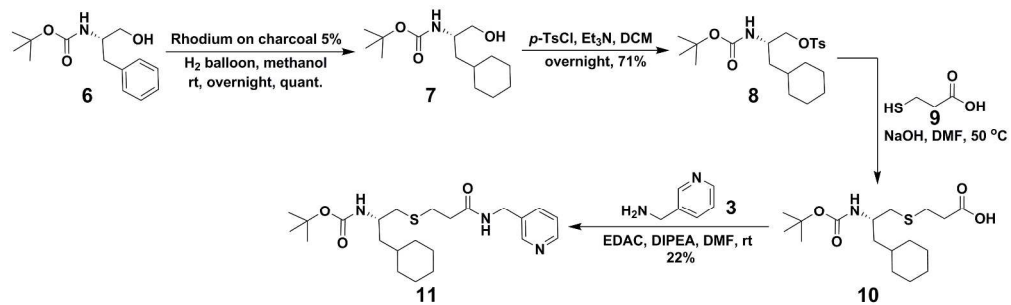
Figure 8. The 1.93 Å crystal structure of CYP3A4 K282A/E285A bound to **4** and imidazole. *A*, Imidazole (in magenta) ligates to the heme, whereas compound **4** binds nearby. The complex is stabilized by two hydrogen bonds (depicted as red dotted lines) established between the carbonyl oxygen and amide nitrogen of **4** and the imidazole nitrogen and Ser119 hydroxyl group, respectively. $2F_o-F_c$ electron density map is contoured at 1σ . *B*, Another view at the active site showing how the pyridine ring of **4** is

1
2
3 positioned relative to the phenylalanine cluster (residues 108, 213, 215, 241 and 304).
4
5 C, Superposition of the **4**- and GS3-bound structures (in green and magenta,
6
7 respectively). H-bonds to Ser119 are shown as red dotted lines.
8
9

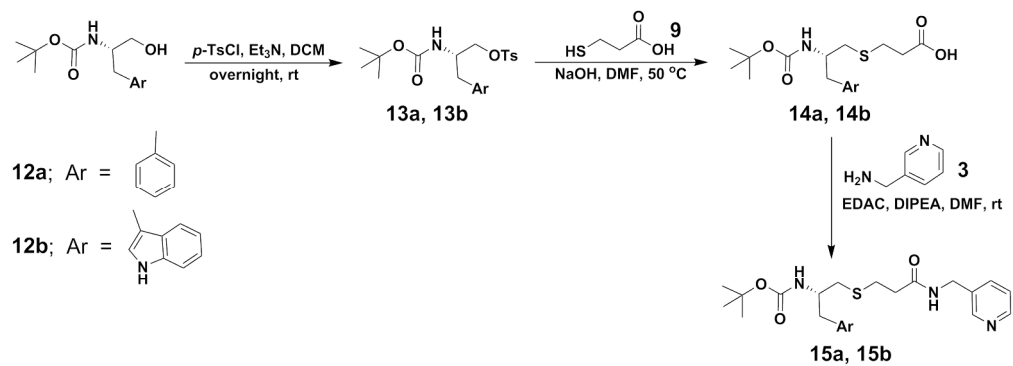
10
11
12 **Figure 9.** The 2.25 Å crystal structure of CYP3A4 K282A/E285A ligated to **4**. A,
13
14 Compound **4** directly binds to the heme *via* the pyridine nitrogen. The **4** backbone
15
16 bends in order to place the end portion into the P2 site. $2F_o - F_c$ electron density map is
17
18 contoured at 1σ . B, Superposition of the **4**- and GS3-bound structures reveals that,
19
20 similar to **15a** and **15b**, compound **4** rotates around the pyridine nitrogen by $\sim 180^\circ$ to
21
22 optimize hydrophobic interactions at the P2 site through the aliphatic backbone and *Boc*
23
24 moiety.
25
26
27
28
29
30
31
32
33
34
35
36
37
38
39
40
41
42
43
44
45
46
47
48
49
50
51
52
53
54
55
56
57
58
59
60



scheme 1
245x71mm (300 x 300 DPI)



scheme 2
252x76mm (300 x 300 DPI)



scheme 3
236x85mm (300 x 300 DPI)

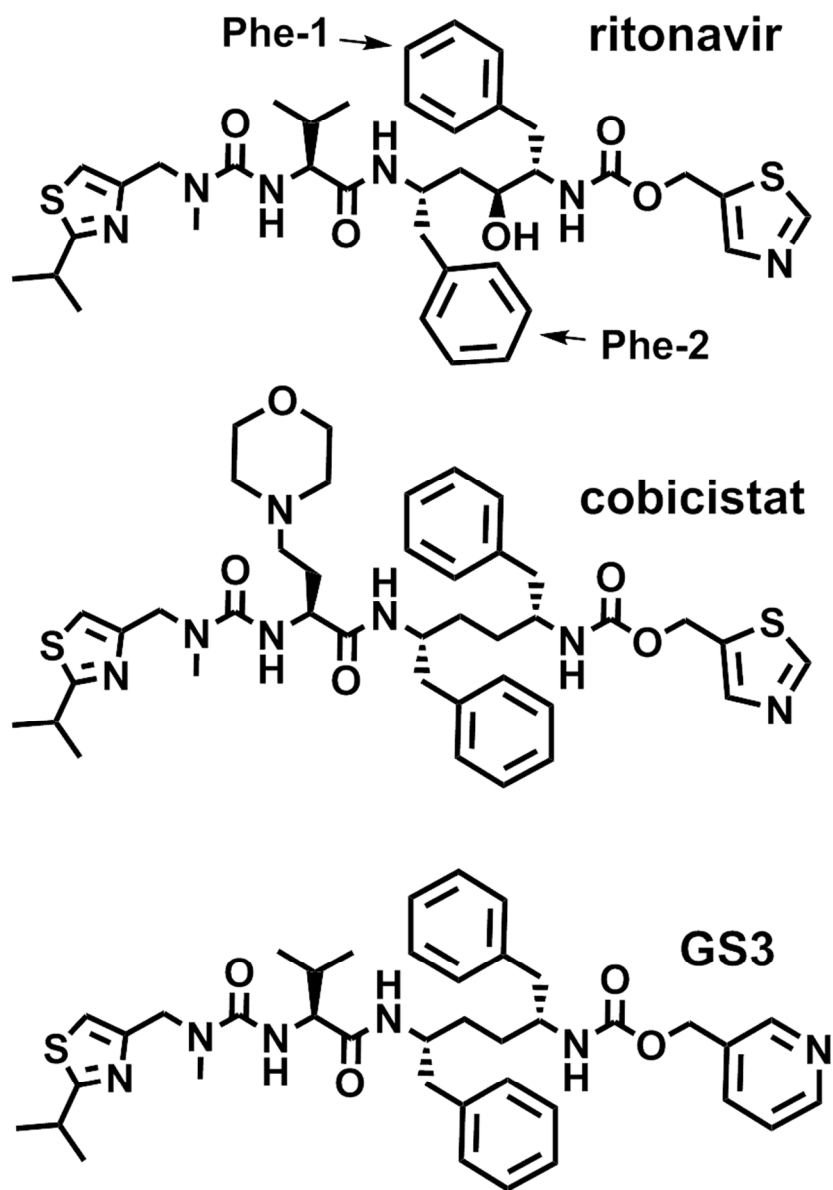


figure 1
73x104mm (300 x 300 DPI)

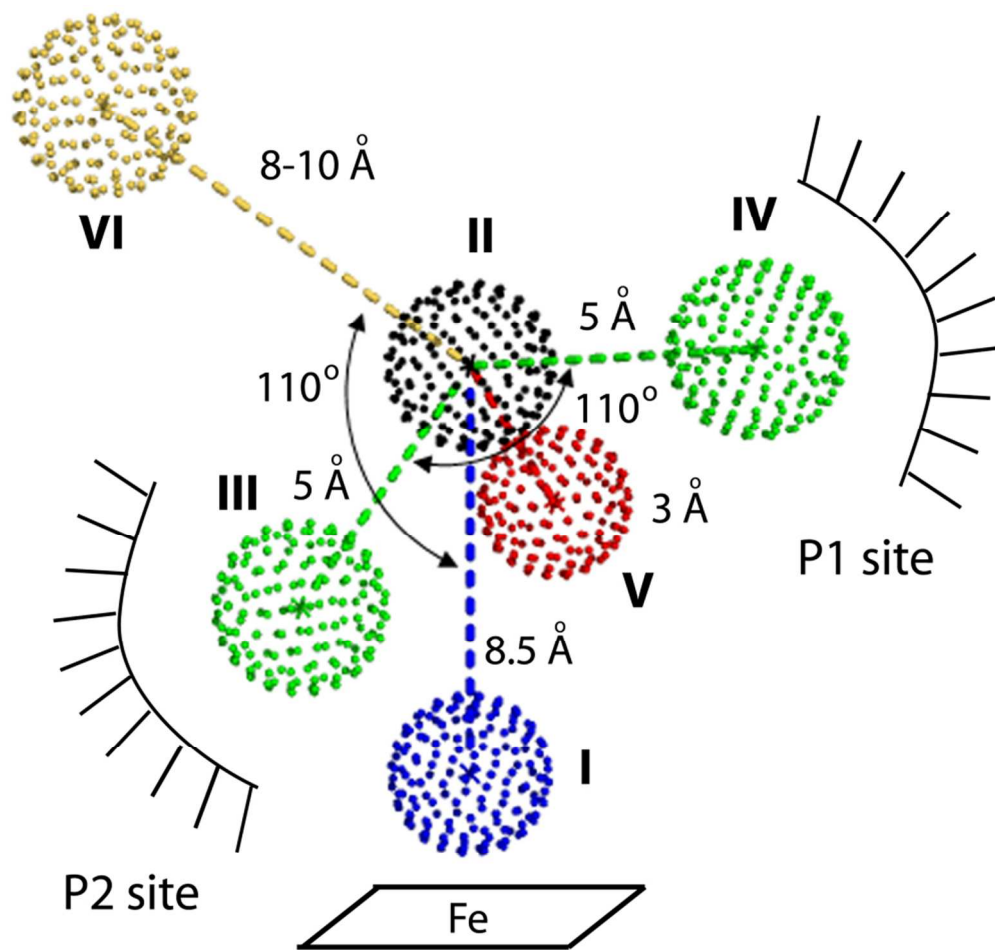


figure 2
84x80mm (300 x 300 DPI)

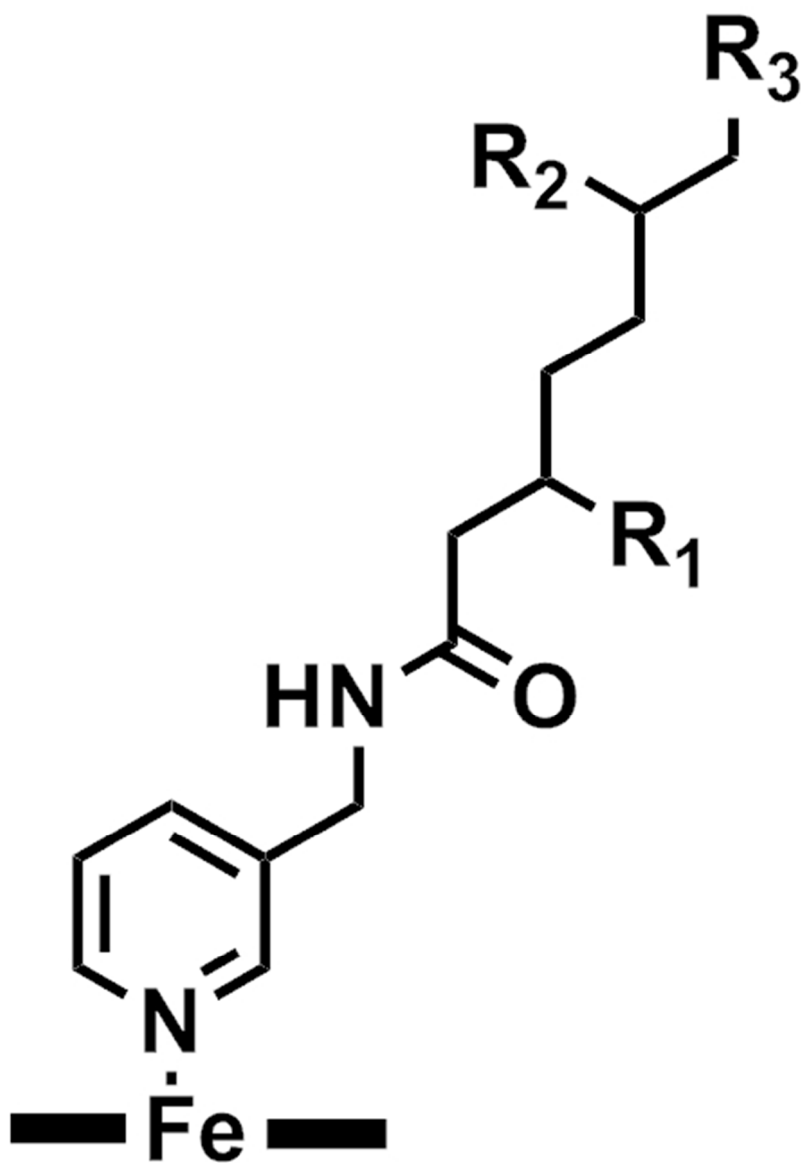


figure 3
38x56mm (300 x 300 DPI)

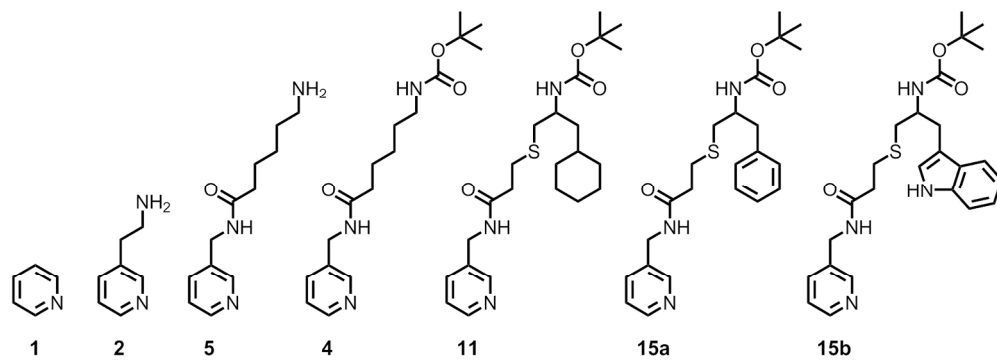


figure 4
167x59mm (300 x 300 DPI)

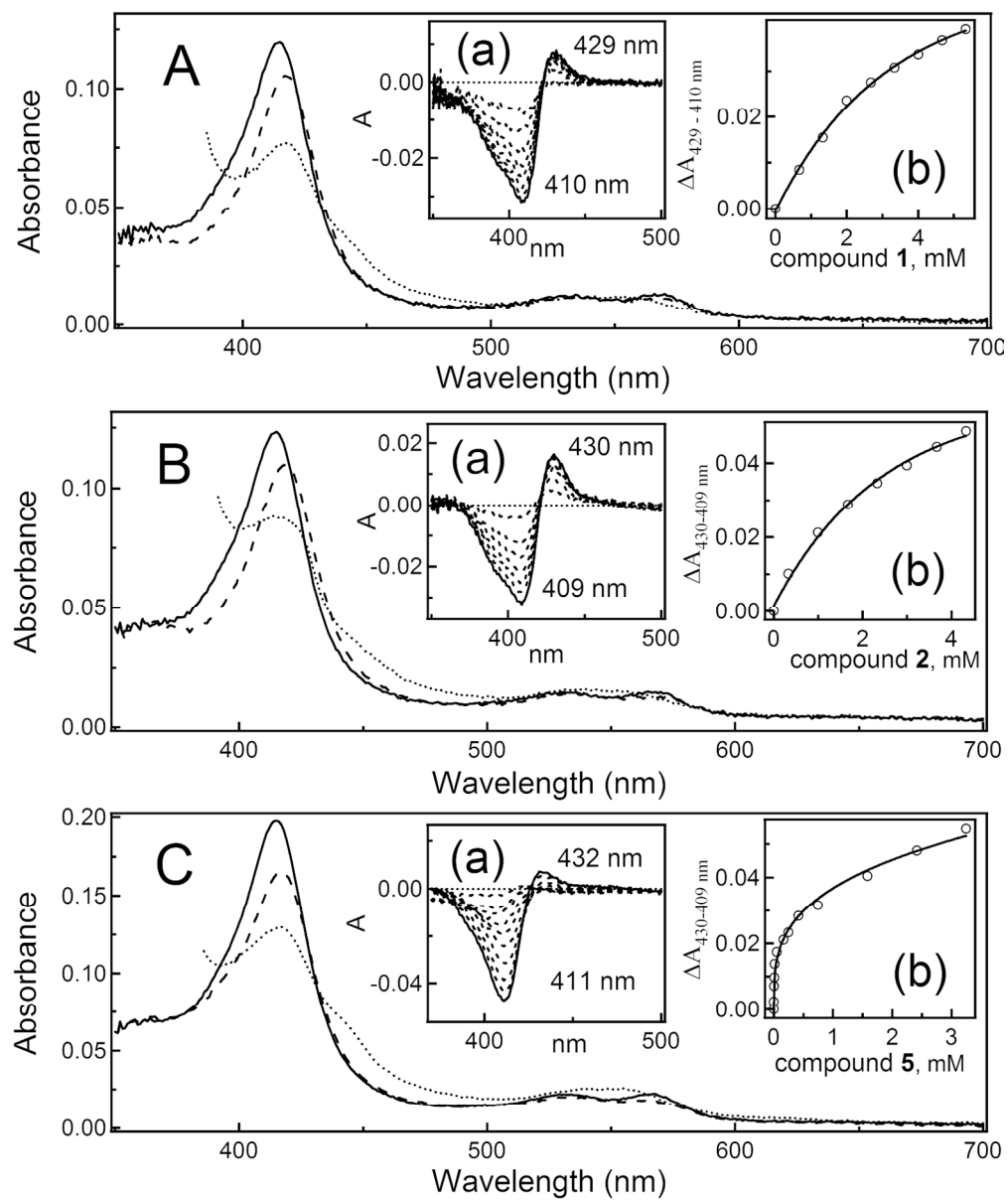


figure 5
137x164mm (300 x 300 DPI)

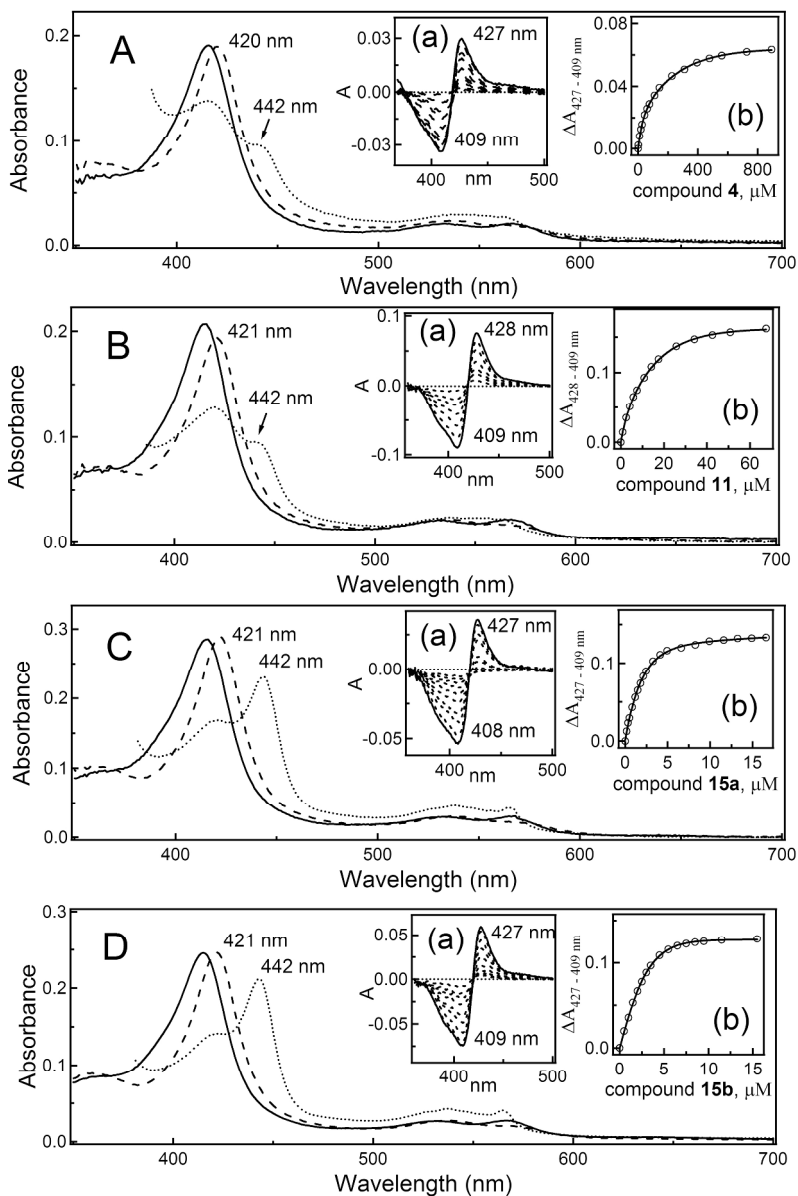


figure 6
219x333mm (300 x 300 DPI)

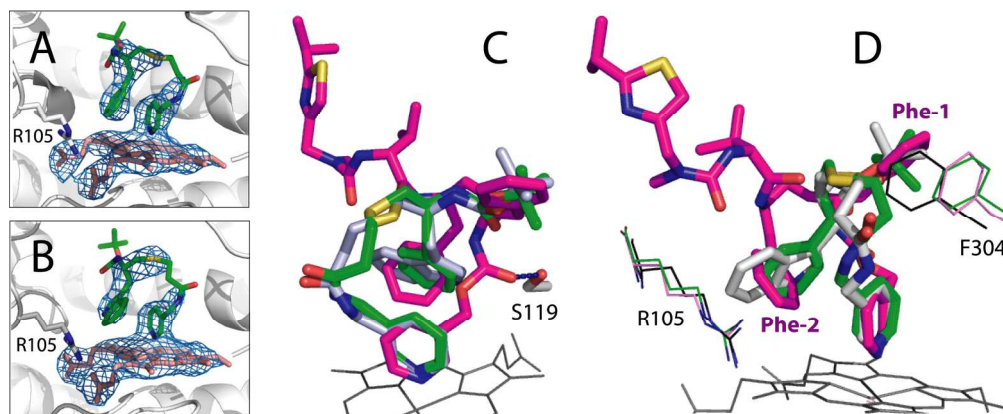


figure 7
177x73mm (300 x 300 DPI)

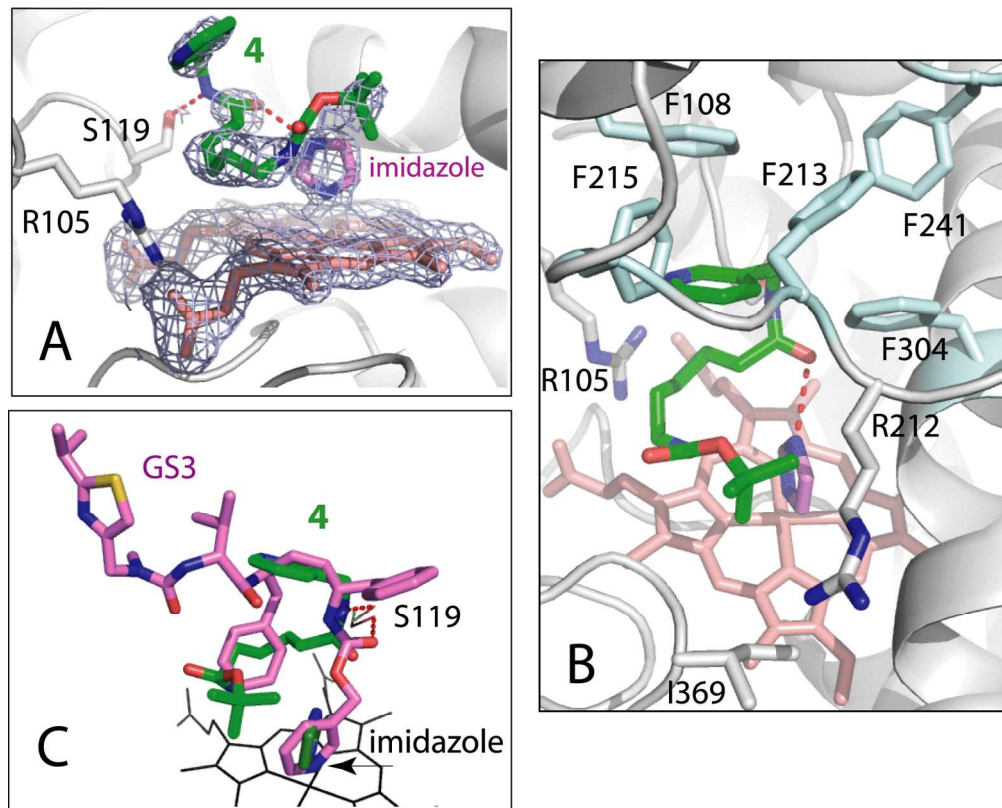


figure 8
148x119mm (300 x 300 DPI)

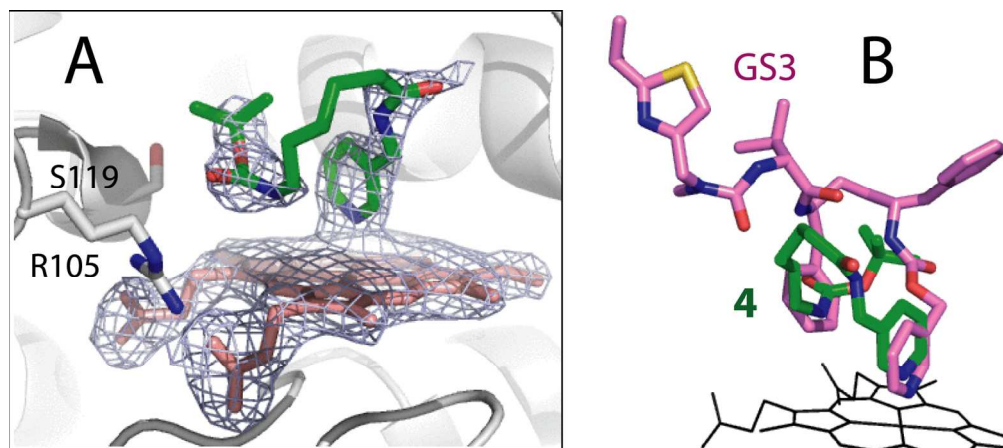


figure 9
144x64mm (300 x 300 DPI)

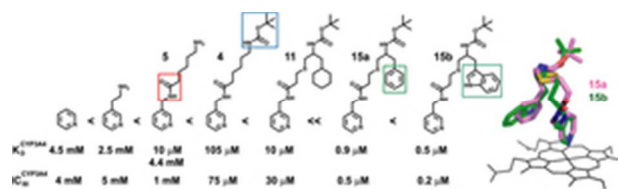


Table of Contents figure
25x7mm (300 x 300 DPI)